energy&fuels

Article

pubs.acs.org/EF

# New Two-Dimensional Particle-Scale Model To Simulate Asphaltene Deposition in Wellbores and Pipelines

Aliakbar Hassanpouryouzband,*[,†,‡] Edris Joonaki,[†] Vahid Taghikhani,[‡,§] Ramin Bozorgmehry Boozarjomehry,[‡] Antonin Chapoy,[†,∥] and Bahman Tohidi[†]

[†]Hydrates, Flow Assurance & Phase Equilibria Research Group, Institute of Petroleum Engineering, School of Energy, Geoscience, Infrastructure and Society, Heriot-Watt University, Riccarton, Edinburgh EH14 4AS, United Kingdom

[‡]Chemical and Petroleum Engineering Department, Sharif University of Technology, Post Office Box 11365-9465, Tehran, Iran

[§]Department of Chemical and Biomolecular Engineering, Rice University, Houston, Texas 77005, United States

[∥]Centre of Thermodynamics of Processes (CTP), Mines ParisTech, 35 Rue Saint-Honoré, 77305 Fontainebleau, France

Supporting Information

**ABSTRACT:** A new two-dimensional dynamic model was developed to simulate asphaltene precipitation, aggregation, and deposition at isothermal and non-isothermal conditions. The perturbed-chain statistical associating fluid theory equation of state was used to model the asphaltene precipitation. Also, novel kinetic models were used to account for the aggregation and deposition of asphaltene particles. The effect of the aggregate size on the rate of aggregation and deposition was studied, and it was concluded that the rate of asphaltene deposition increases, while the concentration of nanoaggregates increases in the well column. The tendency of smaller aggregates to deposit on the surface could be explained as a result of the increase in the diffusion coefficient of asphaltene aggregates. The results obtained from the new model for the rate and amount of asphaltene deposition were compared to the experimental data reported in the literature. It was shown that the results of the new simulation were in good agreement with the experimental data.

## 1. INTRODUCTION

Asphaltenes are the heaviest, most polar, and most surface-active species of crude oils, which are insoluble in *n*-alkanes (e.g., *n*-hexane and *n*-heptane) and soluble in light aromatics (e.g., toluene and xylene).[1] Asphaltene molecules contain large polycyclic aromatic hydrocarbons with peripheral aliphatic chains, which are embedded with a small amount of heteroatoms, such as sulfur, oxygen, and nitrogen.[2] They also consist of trace moieties of metals (in parts per million), such as iron, nickel, and vanadium, which can appear as porphyrin or non-porphyrin structures.[3] On the basis of asphaltene concentrations in crude oils, the asphaltene molecules are dispersed in the oleic phase with a size range from ∼1.5 to ∼5 nm in width.[4] It is widely believed that the asphaltene nanoaggregates will either flocculate to form larger particles,[5] which can flow through a channel (e.g., pipeline and porous media), or deposit on the surfaces. In many oil reservoirs, asphaltenes are fairly stable in the oil; however, a small variation in the pressure, composition, and temperature can cause asphaltene phase instability and alteration in their solubility parameter,[6,7] and they can precipitate and aggregate out of the crude oil, leading to expensive deposition problems in pipelines, well, valves, and porous media. It is extremely important to identify the flow of precipitated and aggregated asphaltene particles and determine their disposition for deposition. However, because of the complexity of the asphaltene molecular structure and lack of proper knowledge of the asphaltene aggregate deposition process, modeling studies of this undesirable phenomena are scarce. Recent advances in asphaltene science enable us to have a new look at how a reliable asphaltene deposition model can sufficiently predict asphaltene deposition tendencies onto the surfaces and cause a significant positive effect on fluid flow assurance in pipelines and porous media.[8]

Here, a few papers and some of the obtained results from previous asphaltene deposition model studies will be briefly described. The first was authored by Escobedo and Mansoori,[9] who developed an asphaltene deposition model based on models for aerosol (microscopic liquid or solid particles dispersed in air currents) deposition. The model was developed by accounting for both diffusive and convective mechanisms for transport of the asphaltene particle to the pipe wall.[10] Jamialahmadi et al.[11] developed a mechanistic asphaltene deposition model based on three parameters of oil velocity, bulk and surface temperature, and concentration of flocculated asphaltenes. They conducted flow loop experiments to determine the rate of asphaltene deposition by measurement of the thermal resistivity of the asphaltene deposit. They proposed an Arrhenius-type equation for adhesive force between flocculated asphaltenes and the metal surface, ignoring the effect of the particle size distribution of precipitated asphaltenes. The model developed by Jamialahmadi was then used by Soulgani et al.[12] for predicting asphaltene deposition in an oil reservoir. They matched the experimental asphaltene

**Special Issue:** 18th International Conference on Petroleum Phase Behavior and Fouling

**Received:** September 11, 2017
**Revised:** November 9, 2017
**Published:** November 9, 2017






DOI: 10.1021/acs.energyfuels.7b02714
*Energy Fuels* 2018, 32, 2661−2672

deposition rate with a correlation based on the aforementioned Arrhenius exponential term with an assumption that the chemical reaction mechanism controlled the asphaltene deposition onto the tubing surface. There is no validation for the proposed deposition mechanism. Ramirez-Jaramillo et al.[13] proposed the application of a molecular diffusion model to describe the transportation of asphaltene aggregates to the wall. They claimed that the net rate of asphaltene deposition is the difference between the rate of deposition and removal of asphaltene. These researchers employed Fick's law for molecular diffusion, accounting for the rate of deposition and the Kern and Seaton[14] model for expressing the removal of asphaltene deposition. They also considered that the asphaltene aggregate concentration gradient was due to the wall temperature gradient. This modeling methodology was inspired from a well-developed hypothesis for wax deposition by Burger et al.,[15] which is unfortunately not in agreement with laboratory data obtained by Greaves et al.[16] Their experimental data on asphaltene deposition using a Couette device revealed that the wall temperature gradient did not cause a significant effect on the asphaltene deposition rate. Eskin et al.[17] developed an asphaltene deposition model based on particle flux mass transfer expressions in turbulent flows. They assumed a population balance model for asphaltene particle size distribution over the pipe cross section and Brownian diffusion for transport of aggregated asphaltenes to the wall surface. The model had three tuning parameters, which were obtained by conducting laboratory tests with a Couette device, while thermodynamics of asphaltene precipitation from bulk solution was not addressed. The asphaltene deposition model of Vargas et al.[18] consists of several submodels explaining the asphaltene precipitation, aggregation, transport, and deposition onto the wall surface. The pseudo-first-order reactions were used to model the asphaltene aggregation and deposition steps. The particle transport was defined by the convection−diffusion equation. The diffusivity of asphaltene aggregates in fluid flow through a pipe was considered to be fixed and approximately equal to the determined diffusivity of asphaltene particles in toluene. The model included different tuning parameters that had to be identified on the basis of experimental data. Hashmi et al.[19] introduced a new asphaltene deposition model, which proposes that asphaltene deposition onto the metal surface is governed by a diffusion-driven mechanism. Asphaltene deposition and clogging were assessed by injecting precipitating petroleum fluid mixtures into a capillary tube. The agreement was found between model predictions and experimental data. However, the model was only developed for laminar flow, and further investigation is required to verify the model in the more real condition of fluid flow along a pipe or wellbore. Vilas Bôas Fávero et al.[20] proposed a new device to investigate the asphaltene deposition phenomenon. The apparatus was made of a packed bed of stainless-steel beads over which a solution of crude oil−alkane is flown, and the asphaltene deposit is well-monitored. The experimental results prove the use of the advection−diffusion equation to model asphaltene deposition. They matched the obtained asphaltene deposition profile along the packed bed with theoretical behavior predicted by the diffusion-limited correlations for mass-transfer deposition.

A review of the existing literature reveals that there is a lack of a comprehensive deposition simulator that fully considers all effective parameters. These parameters are thermodynamics of asphaltene precipitation, aggregation of precipitated nanoscale particles, and finally the transport of particles to the surface and deposition of particles.

In this work, a novel framework was developed to predict the deposition profile of asphaltenes along the flow of a multiphase fluid from the wellbore to the wellhead. In this model, the perturbed-chain statistical associating fluid theory (PC-SAFT) equation of state (EoS) was used to study the stability of oil/asphaltene mixtures. A new classification for the particle size of precipitated asphaltenes was also presented to describe Newton's second law. The Smoluchowsky[21] aggregation kinetic model was used to account for the self-association of asphaltenes. A modified submodel was also developed for the asphaltene deposition term. The advection−diffusion equation (ADE) in a cylindrical coordinate was used to track the transport of asphaltene particles in both axial and radial directions. A numerical scheme was applied to solve all governing partial differential equations (PDEs) simultaneously. The results obtained from the new model was compared and validated against experimental data of asphaltene deposition in the capillary tube to show the robustness of the model.

## 2. MODEL DEVELOPMENT

**2.1. Thermodynamic Modeling.** The PC-SAFT EoS has been one of the most reliable equations of state that was proposed for non-associating fluids by applying the perturbation theory of Barker and Henderson[22] for dispersive interactions within the PC-SAFT model. A simple approximate solution for a given molecular model is typically described using perturbation theories. Originally, the PC-SAFT assumed the hard-sphere fluid as a reference fluid and was developed for spherical molecules. In this methodology, the total intermolecular forces are divided into reference and perturbation terms. The hard-chain fluid with high attractive intermolecular forces is assumed as the reference fluid in the model. This model needs three parameters of each non-associating and nonpolar components, which are the segment number in the molecule ($m$), the segment diameter ($\sigma$), and the interaction energy between each molecular segment $\varepsilon/k$ to model both phase equilibria and bulk properties of the hydrocarbon mixtures. These parameters are related to the average molecular weight of the component and are determined commonly by simultaneously fitting the PC-SAFT EoS to the measured saturated liquid density, speed of sound, heat capacity, and vapor pressure data of the components. A modified square well potential for the segment of a chain is assumed within the PC-SAFT EoS, which describes the residual Helmholtz free energy of a mixture of non-associating fluids. In the framework of the PC-SAFT proposed by Gross and Sadowski,[23] the residual Helmholtz free energy is separated into the hard-chain reference fluid and the dispersion contribution.

$$\tilde{a} = \tilde{a}^{\mathrm{hc}} + \tilde{a}^{\mathrm{disp}} \tag{1}$$

The compressibility factor can be derived using the following thermodynamic relation:

$$Z = 1 + \eta_{\mathrm{p}}\left(\frac{\partial \tilde{a}^{\mathrm{res}}}{\partial \eta_{\mathrm{p}}}\right)_{T,x_i} \tag{2}$$

The pressure can be calculated in units of Pa = N/m$^2$

$$P = Zk_{\mathrm{B}}T\rho_{\mathrm{n}}\left(10^{10}\,\frac{\text{Å}}{\mathrm{m}}\right)^3 \tag{3}$$

where Å is angstrom (unit of length). From eqs 1 and 2, it is

$$Z = 1 + Z^{\mathrm{hc}} + Z^{\mathrm{disp}} \tag{4}$$

The fugacity coefficient can be related to chemical potential by

$$\ln \varphi_k = \mu_k^{\mathrm{res}}(T, \nu_{\mathrm{v}})/kT^{-\ln Z} \tag{5}$$



DOI: 10.1021/acs.energyfuels.7b02714
Energy Fuels 2018, 32, 2661−2672

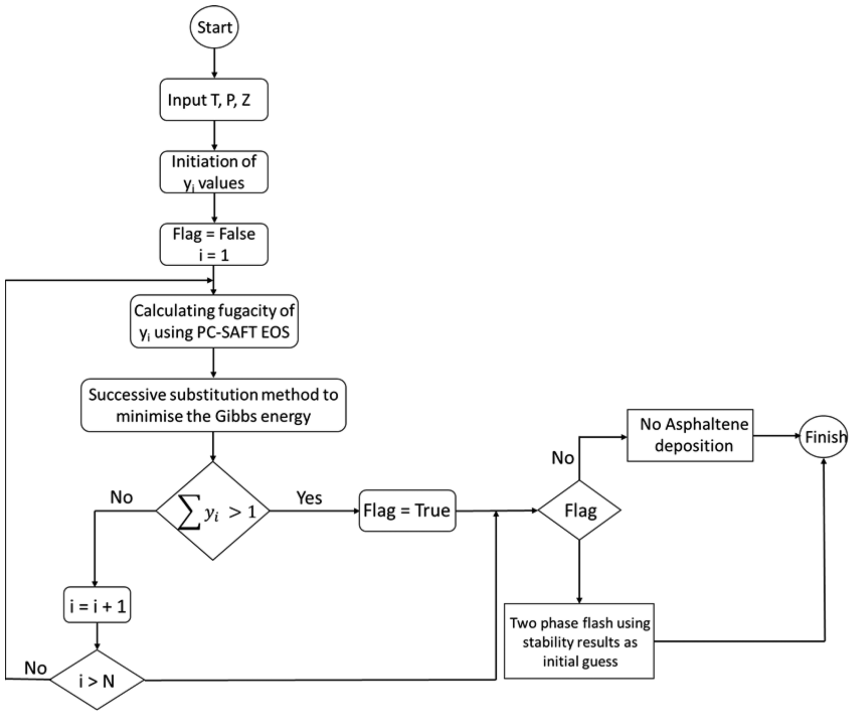


**Figure 1.** Flowchart of the flash algorithm used to study the stability of asphaltene−oil mixtures.

The chemical potentials for different components are derived from eq 6.

$$\mu_k^{\mathrm{res}}(T, \nu_v)/kT = \tilde{a}^{\mathrm{res}} + (Z-1) + \left(\frac{\partial \tilde{a}^{\mathrm{res}}}{\partial x_k}\right)_{T,v,x_i\neq x_k} - \sum_{j=1}^{N}\left[x_j\left(\frac{\partial \tilde{a}^{\mathrm{res}}}{\partial x_j}\right)_{T,v,x_{i\neq x_j}}\right] \quad (6)$$

To perform the stability analysis and flash calculations, the fugacity coefficients are needed. The stability/flash calculation is then used for modeling pressure, volume, and temperature ($PVT$) dependency experiments to obtain thermodynamic results from the EoS. This was schematically represented in Figure 1. Different asphaltene compositions in mixtures were tested using the stability analysis based on the tangent plane distance concept[24] to study the thermodynamics of asphaltene particles in the oil phase corresponding to the global minimum of the Gibbs energy of the mixture. It should be stated that, if the asphaltene phase was stable in the oil, the result of stability analysis would be used as the initial guess composition to conduct the flash calculation. More details on the stability analysis applied here can be found elsewhere.[25−27]

Figure 1 shows the details of thermodynamic calculations of the oil−asphaltene system studied in this work. As explained, for each non-associating species, the PC-SAFT EoS requires three parameters. To characterize the oil, these three parameters should be determined for each pseudo-component. The parameters were found based on the saturates, aromatics, resins, and asphaltenes (SARA) analysis of the oil, density of stock tank oil, bubble point, and live oil composition of the mixture. Correlations for the three PC-SAFT parameters were previously reported as a function of the molecular weight for paraffins, benzene derivatives, and aromatics. These results were directly used to fit parameters for each component, except for the asphaltene component. The PC-SAFT parameters for asphaltene were fitted by matching the measurements of the asphaltene onset point with model predictions.[28]

**2.2. Viscosity.** A viscosity model based on the correlation developed by Jossi et al.[29] was used to determine the viscosity of the flowing oil containing suspended asphaltene particles. Lohrenz et al.[30] extended the correlation developed by Jossi et al. for computation of the viscosity of hydrocarbons, referred to as the Lohrenz−Bray−Clark (LBC) correlation in the oil and gas industry. The LBC correlation is a fourth-degree polynomial equation in terms of the reduced density as follows:

$$[(\eta - \eta^*)\xi + 10^{-4}]^{1/4} = a_1 + a_2\rho_r + a_3\rho_r^2 + a_4\rho_r^3 + a_5\rho_r^4 \quad (7)$$

where $\eta^*$, $\xi$, and $\rho_r$ are the viscosity of the dilute gas, the viscosity-reducing parameter, and the reduced density, respectively. Constants $a_1$−$a_5$ were reported by Jossi et al.[29] In this work, the Lohrenz et al.[30] mixing rules were used for hydrocarbons. Also, the Brinkman[31] viscosity model was used to calculate the viscosity of a fluid containing a dilute suspension of asphaltene particles given by

$$\mu = \frac{\eta}{(1-\phi)^{2.5}} \quad (8)$$

where $\phi$ refers to the volume fraction of the asphaltene particles.

**2.3. Kinetics of Asphaltene Precipitation.** Once the asphaltene nanoaggregates become unstable in the oil phase, they start precipitating out of the solution at a specific rate. The rate depends upon the difference between the actual concentration of asphaltene in the bulk of oil phase and the equilibrium concentration at the system temperature and pressure. This time-dependent process can be explained by the following first-order reaction equation:

$$R_{\mathrm{per}} = -k_{\mathrm{p}}(C - C_{\mathrm{eq}}) \quad (9)$$

where $C$ is the actual concentration of asphaltene in the oil phase and $C_{\mathrm{eq}}$ is the asphaltene concentration at equilibrium conditions. The factor $k_{\mathrm{p}}$ was considered to be constant in most previously published work[32] on the development of the asphaltene deposition model; however, in this work, an Arrhenius equation type was proposed for $k_{\mathrm{p}}$ as follows:

$$k_{\mathrm{p}} = -k_0 e^{\alpha_{\mathrm{p}}(C - C_{\mathrm{eq}})} \quad (10)$$

Thus, the final equation for the rate of precipitation of unstable asphaltene particles takes the following form:



DOI: 10.1021/acs.energyfuels.7b02714
Energy Fuels 2018, 32, 2661−2672

$$R_{per} = k_0 e^{\alpha_p(C-C_{eq})}(C - C_{eq}) \quad (11)$$

**2.4. Aggregation of Precipitated Asphaltenes.** After precipitation of the asphaltene particles from the bulk of the oil phase, the nanoaggregates tend to stick to each other and form larger aggregates as a result of asphaltene natural self-associating characteristics. The change in the concentration of particles with size $k$ can be modeled using the Smoluchowski[33,34] equation as follows:

$$\frac{dC_k}{dt} = \frac{1}{2}\sum_{i+j=k} K_{ij}C_iC_j - C_k\sum_{i\geq k} K_{ik}C_i \quad (12)$$

where $C_k$ is the concentration of particles with size $k$, in number of particles per cubic meter, and $K_{ij}$ is the collision kernel between $i$ and $j$ particles. For the collision of particles with approximately equal size during the diffusion-limited regime, the collision kernel, $K_{ij}$, can be estimated according to the following equation:[33,34]

$$K_{ij} = \frac{8k_BT}{3\mu}\beta \quad (13)$$

where $T$ is the temperature in kelvin, $K_B$ is the Boltzmann constant in $m^2\ kg\ s^{-2}\ K^{-1}$, $\mu$ is the viscosity in Pa s, and $\beta$ is the collision efficiency.

As experimentally shown, while asphaltene particles smaller than 0.01 $\mu$m were considered as nanoaggregates suspended in the oil phase, asphaltene particles larger than 0.01 $\mu$m can be precipitated when asphaltenes become unstable in the liquid phase.[18]

**2.5. Kinetics of Asphaltene Deposition.** The precipitated asphaltenes start becoming aggregated, and the asphaltene aggregates smaller than 10 $\mu$m[35] move toward the tubing wall as a result of the diffusional forces. In this work, a new equation was proposed to model the asphaltene deposition expressed as

$$R_d = -k_dC^{n_d\mu} \quad (14)$$

where the $R_d$ is the rate of asphaltene deposition, $C$ is the actual concentration of asphaltene, $\mu$ is the viscosity of the oil, and $k_d$ and $n_d$ are two adjustable parameters. It should be noted that the model does not account for possible erosion of previously deposited asphaltene particles, which is currently a limitation of the proposed model. It is also worth mentioning that choosing 10 $\mu$m as the upper limit of the particle size prone to radial diffusion to the wall is an approximation, and further investigation is required to detect the exact quantity.

**2.6. Modeling the Mass and Heat Transfer Processes.** In this study, the cylindrical coordinates were used to simulate the distribution of asphaltene aggregates along an oil well column. A two-dimensional axial−radial flow mass transfer equation was used for the simulation purposes. This type of coordinate was able to track the transport of asphaltenes in both radial and axial directions by considering asphaltene deposition, kinetics of asphaltene precipitation, molecular and eddy diffusion, and also the kinetics of the deposition rate on the surface. The ADE in the cylindrical coordinate is[36]

$$\frac{\partial C}{\partial t} + V_r\frac{\partial C}{\partial r} + V_z\frac{\partial C}{\partial z} + \frac{v_\theta}{r}\frac{\partial C}{\partial \theta} = (D_{wo} + \varepsilon_m)\left[\frac{1}{r}\frac{\partial}{\partial r}\left(r\frac{\partial C}{\partial r}\right) + \frac{1}{r^2}\frac{\partial^2 C}{\partial \theta^2} + \frac{\partial^2 C}{\partial z^2}\right] + R \quad (15)$$

where $R$ is the rate of production and consumption of precipitated asphaltenes, which can be obtained from eq 9, and $D_{wo}$ is the asphaltene diffusivity coefficient in the oil phase. In the present work, the Stokes−Einstein equation with an additional tuning parameter for asphaltene particles has been used to calculate the diffusivity coefficient.[37] This value is given by

$$D_{wo} = f_d\frac{k_BT}{6\pi\mu r_k} \quad (16)$$

where $r_k$ is the radius of particle size $k$ and $f_d$ is the diffusivity tuning parameter. In comparison to advection, transport caused by diffusion in the $z$ direction is very small. Accordingly, diffusion in this direction is neglected. Considering that the precipitated particles only diffuse in the radial direction and assuming the symmetricity in the $z$ direction, eq 15 can be simplified as

$$\frac{\partial C}{\partial t} = -V_z\frac{\partial C}{\partial z} + (D_{wo} + \varepsilon_m)\left[\frac{\partial^2 C}{\partial r^2} + \frac{1}{r}\frac{\partial C}{\partial r} + \frac{\partial^2 C}{\partial z^2}\right] - k_p(C - C_{eq}) \quad (17)$$

where the relation for $R$ was replaced with that in eq 9. The finite difference method (FDM) was used to solve the PDE of eq 17 subject to the following boundary conditions: The concentration of asphaltene at initial time along the wellbore is known and constant.

$$C \text{ at } (t = 0, z, r) = C_0 \quad (18)$$

The concentration of asphaltene in the fluid while entering to the wellbore is constant.

$$C \text{ at } (t, z = 0, r) = C_r \quad (19)$$

The asphaltene concentration change during production at $r = 0$ is zero.

$$\frac{\partial C}{\partial r} \text{ at } (t, z, r = 0) = 0 \quad (20)$$

Deposition occurs at $r = r_w$ according to deposition kinetics.

$$\frac{\partial C}{\partial r} \text{ at } (t, z, r = r_w) = -k_dC_d^{n_d\mu} \quad (21)$$

$C_d$ is the concentration of those asphaltene aggregates that can deposit on the surface. Equation 21 is the key part for modeling the deposit layer formation, where $r_w$ reduces after deposition occurs.

Similarly, for the heat transfer in the cylindrical geometry described in this work, the following equation can be used as[38]

$$\frac{\partial T}{\partial t} + v_r\frac{\partial T}{\partial r} + v_z\frac{\partial T}{\partial z} + \frac{v_\theta}{r}\frac{\partial T}{\partial \theta} = (\alpha_T + \varepsilon_h)\left[\frac{1}{r}\frac{\partial}{\partial r}\left(r\frac{\partial T}{\partial r}\right) + \frac{1}{r^2}\frac{\partial^2 T}{\partial \theta^2} + \frac{\partial^2 T}{\partial z^2}\right] + R \quad (22)$$

where $\alpha_T$ is the thermal diffusivity. The heat generation as a result of change in the asphaltene phase behavior was reported negligible in the literature.[39] In addition, assuming symmetricity along the $z$ axis, eq 22 can be simplified as

$$\frac{\partial T}{\partial t} = -V_z\frac{\partial T}{\partial z} + (\alpha_T + \varepsilon_h)\left[\frac{\partial^2 T}{\partial r^2} + \frac{1}{r}\frac{\partial T}{\partial r} + \frac{\partial^2 T}{\partial z^2}\right] \quad (23)$$

Similar to the mass transfer boundary conditions, the following conditions can be used to solve the PDEs: The fluid temperature is equal to the reservoir temperature while entering the wellbore.

$$T \text{ at } (t, z = 0, r) = T_{res} \quad (24)$$

The fluid temperature is equal to the wellhead temperature while leaving the wellbore.

$$T \text{ at } (t, z = L, r) = T_{WH} \quad (25)$$

The temperature gradient at the center of the wellbore is zero.

$$\frac{\partial T}{\partial r} \text{ at } (t, z, r = 0) = 0 \quad (26)$$

The temperature gradient at $r = r_w$ is equal to the conductive heat transfer from surrounding material

$$\frac{\partial T}{\partial r} \text{ at } (t, z, r = r_w) = \frac{h_o}{k_c}(T_w - T_o) \quad (27)$$

where $h_o$ is the convective heat-transfer coefficient of oil and $k_c$ is thermal conductivity of casing. It should be mentioned that, while the asphaltene layer covers the metal surface, the heat transfer can be affected by the deposition layer, and eq 27 would change to



DOI: 10.1021/acs.energyfuels.7b02714
Energy Fuels 2018, 32, 2661−2672

**Table 1. Classification of Asphaltene Based on Sizes of the Aggregates**

| $i$ (group) | 1 | 2 | 3 | 4 | 5 | 6 | 7 | 8 | 9 | 10 | 11 | 12 |
|---|---|---|---|---|---|---|---|---|---|---|---|---|
| size ($\mu$m) | 0.01 | 0.02 | 0.04 | 0.08 | 0.16 | 0.32 | 0.64 | 1.28 | 2.56 | 5.12 | 10.24 | ≥20.48 |

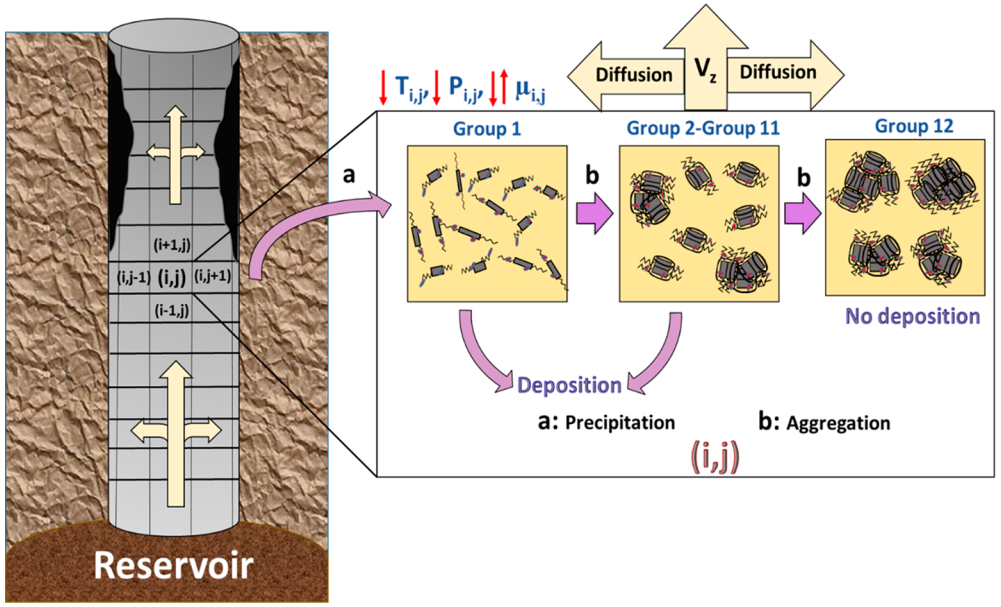


**Figure 2.** Schematic of precipitation, aggregaion, and deposition of asphaltene during the production from the reservoir to wellhead.

$$\frac{\partial T}{\partial r} \text{ at } (t, z, r = r_w) = \frac{h_o}{k_{As}}(T_w - T_o) \tag{28}$$

where $k_{As}$ is the thermal conductivity of asphaltene.

**2.7. Size Classification of Precipitated Asphaltene Particles.** As discussed in section 2.3, it was assumed that asphaltene nanoaggregates start precipitating out of the liquid phase at the size greater than 0.01 $\mu$m. After formation of asphaltene precipitates, the aggregation as a result of diffusional force between the particles starts, which accounts for the distributed asphaltene particle size. To solve the aforementioned heat and mass transfer PDEs, it is required to characterize and classify this distribution. In this regard, the asphaltene particles were classified into 12 groups presented in Table 1.

Using the Smoluchowski[21] equation and considering the generation and consumption of asphaltene particle size, the rate of change in the concentration of each asphaltene aggregate size can be modeled as

for $i = 1$

$$\frac{\partial C_i}{\partial t} = \left[\frac{\partial C}{\partial t} + k_p(C - C_{eq})\right]\frac{C_i}{C} - KC_i^2 - k_p(C - C_{eq}) \tag{29}$$

For $i = 1$, the term of particle generation as a result of smaller asphaltene aggregates is zero.

for $i = 2-11$

$$\frac{\partial C_i}{\partial t} = \left[\frac{\partial C}{\partial t} + k_p(C - C_{eq})\right]\frac{C_i}{C} + \frac{1}{2}KC_{i-1}^2 - KC_i^2 \tag{30}$$

for $i = 12$

$$\frac{\partial C_i}{\partial t} = \left[\frac{\partial C}{\partial t} + k_p(C - C_{eq})\right]\frac{C_i}{C} + \frac{1}{2}KC_{i-1}^2 \tag{31}$$

In contrast to particle size $i = 1$, the term $KC^2$ is zero for $i = 12$ because there is no larger asphaltene aggregate than the aggregates in the aggregate group with $i = 12$ in our classification.

For $C$ in eq 15, we have

$$C = \sum_{i=1}^{12} C_i \tag{32}$$

It should be noted that it was assumed that asphaltene particles just aggregate in a step-by-step process. It means that the aggregates with size number $i$ further flocculate to reach the aggregate size $i + 1$ or may break and become the aggregate with size $i - 1$.

The asphaltene nanoaggregates are stable and soluble in crude oil at reservoir conditions. However, as shown in Figure 2, when the crude oil moves up from the reservoir to the wellhead along the wellbore, the pressure, temperature, and viscosity of the oil change. As a result of alterations in these conditions, the asphaltene nanoaggregates, which are dissolved in the solution, become unstable and separate out of the crude oil. This step of generation of primary aggregates is called asphaltene precipitation (group 1). Then, some of the precipitated asphaltene particles are moved along the wellbore with the oil flow, and some of them might be deposited onto the surface. These primary asphaltene aggregates can also interact with each other and form larger particles through the aggregation process (groups 2–11). Again, some of these secondary asphaltene aggregates may deposit, and some of them continue the aggregation process and make bigger aggregates (group 12), which are carried along with the oil flow and cannot deposit onto the walls.

**2.8. Change in Pressure and Fluid Velocity along the Flow.** As the fluid flows along the tubing, its pressure changes resulting from friction, gravity, and also velocity variation. In this study, the Darcy-Weisbach[40] equation was used to predict the pressure loss during flow in the pipeline, as expressed below

$$\Delta P = g\rho\Delta z + \frac{\rho}{2}\Delta v^2 + \frac{2f_F\rho v^2 L}{D} \tag{33}$$

where the friction factors in the pressure loss as a result of friction in both laminar and turbulent flow can be calculated as

for laminar flow

$$f_F = \frac{16}{N_{Re}} \tag{34}$$



DOI: 10.1021/acs.energyfuels.7b02714
Energy Fuels 2018, 32, 2661−2672

for turbulent flow

$$\frac{1}{\sqrt{f_F}} = -4\log\left\{\frac{\varepsilon}{3.7065} - \frac{5.0452}{N_{Re}}\log\left[\frac{\varepsilon^{1.1098}}{2.8257} + \left(\frac{7.149}{N_{Re}}\right)^{0.08981}\right]\right\} \quad (35)$$

where $\varepsilon$ is the relative roughness. The velocity distribution of the fluid flow inside the pipeline for laminar flow can be related to the pressure difference across the pipe, and with incorporation of the Poiseuille equation inside the tube, the following equation can be obtained:[41]

$$V_z = \frac{\Delta P R^2}{4\mu L}\left[1 - \left(\frac{r}{r_w}\right)^2\right] \quad (36)$$

where $r_w$ is the capillary/wellbore radius, which will be reduced after asphaltene deposition. For turbulent flow, the modified law of the wall can efficiently predict the radial velocity profile[42] and can be expressed as follows:

$$V_z = V_z^+\sqrt{\frac{\tau_w}{\rho}} \quad (37)$$

where $V_z^+$ and $\tau_w$ refer to dimensionless velocity and shear stress at the wall, respectively, and are calculated by

$$V_z^+ = \begin{cases} r^+ & r^+ \le 5 \\ 5\ln r^+ - 3.05 & 5 \le r^+ \le 30 \\ 2.5\ln r^+ + 5.5 & 30 < r^+ \end{cases} \quad (38)$$

$$\tau_w = f_F\frac{\rho v^2}{8} \quad (39)$$

where $r^+$ is the dimensionless distance and is given by

$$r^+ = \frac{r_w - r}{v_\mu}\sqrt{\frac{\tau_w}{\rho}} \quad (40)$$

where $v_\mu$ is the kinematic viscosity.

The most important basic processes occurring in an asphaltene deposition simulation for a defined well were schematically illustrated in Figure 3. It should be noted that Figure 3 gives a simplified picture because, in practice, many more detailed processes came into play. The simulation loop was sustained by a combination of three main parts, i.e., thermodynamic packages, dynamic packages, and data analysis, as expounded in Figure 1. In addition, as seen from Figure 3, the geometry of the flow area changes once the amount of asphaltene deposition changes with time. This will, in turn, change fluid flow dynamics in the wellbore, causing change in the amount of precipitated asphaltene along the wellbore during the production time. The numerical method for solving eqs 17 and 23 was provided in the Supporting Information.

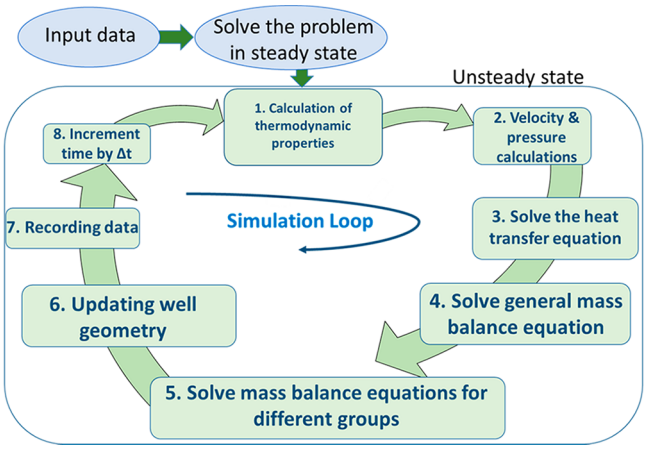


**Figure 3.** Typical simulation loop. Each step begins with the thermodynamic calculation part, continues with mass and heat transfer calculations, geometry section, and data recording, and ends with time update.

## 3. RESULTS AND DISCUSSION

**3.1. Example of an Asphaltene Deposition Simulation.** The following parameter set was used to model the asphaltene deposition in a well column. The sample well data and all other parameters required for modeling were listed in Table 2.

**Table 2. Parameters Used in the Modeling of Asphaltene Deposition**

| parameter | value |
|---|---|
| well depth (m) | 4572 |
| production string diameter (cm) | 3.492 |
| earth temperature gradient (K/m) | 0.0271 |
| $P_{res}$ (MPa) | 35.594 |
| $P_{WH}$ (MPa) | 10.466 |
| $T_{res}$ (K) | 427.594 |
| $T_{WH}$ (K) | 307.95 |
| $K_c$ (W m$^{-1}$ K$^{-1}$) | 50 |
| $\alpha_T$ (m$^2$/s) | $9.8 \times 10^{-7}$ |
| $f_d$ | $1.81 \times 10^2$ |
| $\beta$ | 0.68 |
| $k_0$ (s$^{-1}$) | $3.14 \times 10^{-2}$ |
| $\alpha_p$ (cm$^3$/g) | $8.19 \times 10^2$ |
| $k_d$ (s$^{-1}$) | $6.18 \times 10^{-4}$ |
| asphaltene content of the deposits (%) | 45 |

As mentioned before in the structure of the new asphaltene deposition model, the thermodynamic characterization of the crude oil was one of the very first steps to achieve an accurate and reliable thermodynamic model at various temperatures and pressures. The results of the thermodynamic model were then used as input data for the asphaltene deposition model developed in this study. The crude oil composition was obtained elsewhere.[28] The crude oil thermodynamic properties, such as saturation pressure and asphaltene onset pressures for various temperatures, and the dead oil SARA analysis data were obtained from Panuganti et al.[28] A detailed explanation of the characterization procedure and the PC-SAFT parameters used in this work are available in the literature.[43,44] The oil density was reported to be about 36−40° American Petroleum Institute (API) gravity. The oil characterization was conducted to match the given density range, and the PC-SAFT prediction result was 38° API gravity. The effect of the temperature on the saturation pressure of the crude oil is shown in Figure 4. The black solid diamond data points in Figure 4 are the experimentally determined bubble point pressure data from Panuganti et al.[28] The black dash dot line in Figure 4 is the PC-SAFT prediction of the bubble pressure for various temperatures, and as observed, the PC-SAFT predictions match very well with the experimental measurements. The triangle data points represent the experimentally determined asphaltene upper onset pressure for different temperatures. The black solid line represents the PC-SAFT predictions. It should be noted that the PC-SAFT


DOI: 10.1021/acs.energyfuels.7b02714
Energy Fuels 2018, 32, 2661−2672

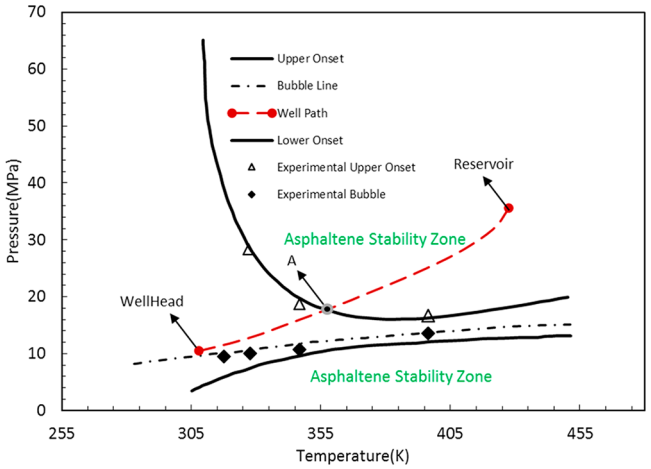


**Figure 4.** Asphaltene phase behavior at different pressures and temperatures for the crude oil investigated in this study.

predictions match the experimental data very well when the reported onset values are compared to the simulation results. The wellbore operating conditions are shown from the reservoir to the wellhead by the long dash line. The black round dot line represents the PC-SAFT prediction of the lower asphaltene precipitation onset pressure curve. The region between the upper asphaltene onset pressure and the lower onset pressure curves makes the asphaltene precipitation region. The crude oil is stable in terms of asphaltene precipitation above this region. As the crude oil flows upward along the wellbore, the pressure and temperature decreased, as observed from the long dash line, and the crude oil goes into the asphaltene precipitation region, where the asphaltene particles start coming out of the solution (point A). This phenomenon continuously takes place until the bubble line, after which the light components of the crude oil begin separating out of the solution. Because of the removal of these light components from the crude oil, which are themselves appropriate precipitating agents for asphaltene particles, the crude oil becomes a more suitable solvent for asphaltenes, and therefore, the asphaltene particles again become stable in crude oil below the lower asphaltene onset pressure curve. The obtained pressure and temperature data were matched to the wellbore depth, and this information was used to determine the thermodynamic stability of asphaltenes in crude oil along the wellbore depth. This was significant input data for the modeling of asphaltene deposition.

Temperature and pressure information is crucial for modeling and is fundamentally related to asphaltene deposition, forward predictions, and reservoir and borehole stability analysis. Figure 5 shows temperature and pressure profiles along the wellbore. Temperature and pressure effects were basically identified as a major cause of changes in asphaltene precipitation and deposition. Figure 5 presents a typical temperature profile for the borehole wall, which is different from the formation temperature. This difference depends upon the heat transfer properties of casing material in the presence of asphaltene deposition. A pressure-depth profile in a well drilled in a field under production is also presented in Figure 5. The pressures in and out of the asphaltene stability zone have been affected by vertical flow through the reservoir and also asphaltene precipitation and deposition. The measured gradients reflect the pressure drop created by the vertical flow.

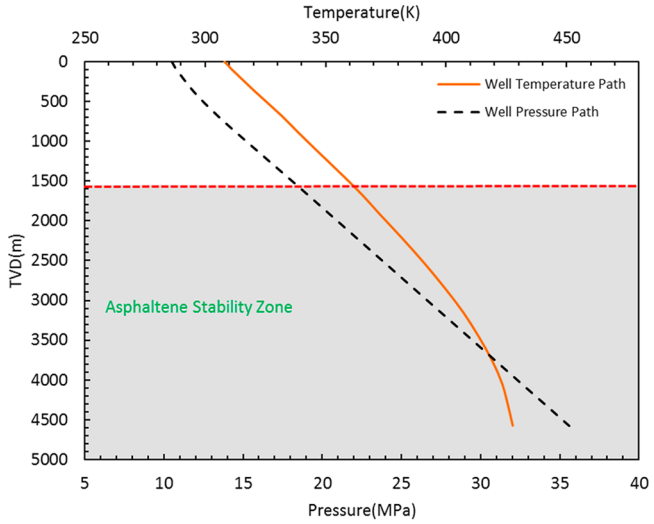


**Figure 5.** Well temperature and pressure profiles along the TVD in two asphaltene stable and asphaltene unstable regions.

A higher asphaltene content in crude oil causes additional problems related to oil transportation and processing because of an increase in oil viscosity as a result of the presence of more asphaltenes. Our modeling results on oil viscosity and true vertical depth (TVD) in wellbore affecting the crude oil viscosity are plotted in Figure 6.

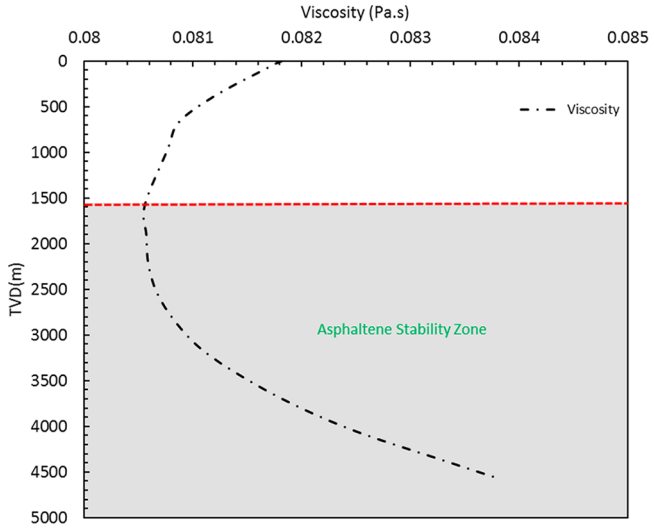


**Figure 6.** Viscosity variation with the TVD in two asphaltene stable and asphaltene unstable regions.

The viscosity of the crude oil increases as a result of the presence of precipitated asphaltene aggregates. This increase became significant at and after the asphaltene flocculation onset and, therefore, could be used to determine the asphaltene precipitation onset points. Oil compositional grading as a result of asphaltene precipitation along the wellbore was an undeniable phenomenon, and with asphaltene compositional changes, the crude oil viscosity varied considerably with the TVD. The asphaltene deposition could be reliably predicted, characterized as a highly oil viscous zone with a high asphaltene content, using a modeling study of the crude oil viscosity changes with depth because of asphaltene compositional grading.


DOI: 10.1021/acs.energyfuels.7b02714
Energy Fuels 2018, 32, 2661−2672

Using appropriate kinetic parameters presented in Table 2 and also employing the thermodynamic model explained in the previous sections, the asphaltene deposition model was developed. Figure 7 shows the variation of asphaltene deposition thickness in different TVDs at various time periods. As seen from this figure, the time-dependent deposition thickness increases over time in the studied well column. After 9 months, a larger segment of the well column will be exposed to the asphaltene deposition. Also, it can be observed that, at the depth of nearly 1600 m, the asphaltene in the system started depositing, where the pressure of the system fell below the upper asphaltene onset pressure and the thickness reached a maximum amount at the depth of nearly 800 m. The reduction in the distance between the graphs with respect to time, as given in Figure 7, indicates that the asphaltene deposition rate decreases over time. This could be plausibly justified by the fact that, upon depositing more asphaltene on the tubing wall at constant bottomhole and wellhead pressures, a reduction in the flow area and, consequently, a reduction in the flow rate (eq 33) can happen, which, in turn, can lead to a less asphaltene flow, causing a decrease in the asphaltene deposition rate. In addition, a change in the wellbore radius and flow rate of the fluid can change the pressure−temperature conditions of the fluid, altering the thermodynamic properties of the fluid along the wellbore. This effect can be clearly observed from Figure 8, which will be discussed.

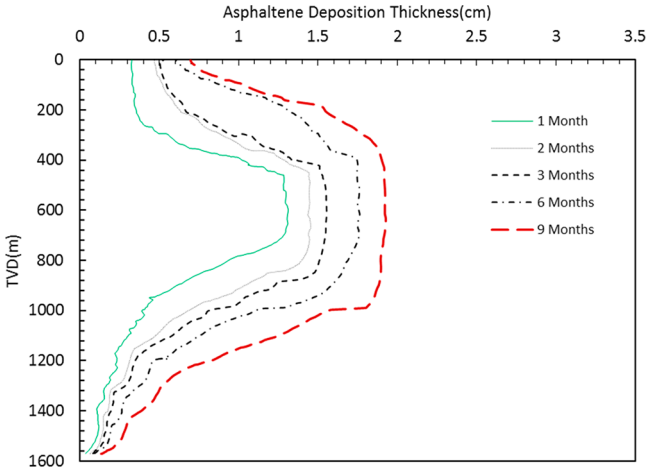


**Figure 7.** Asphaltene deposit layer thickness distribution along the depth of the wellbore for different production times.

Figure 8 shows the amount of destabilized and suspended asphaltene particles in the bulk of flow throughout the well column at various time periods. As seen from this figure, the asphaltene particles dissolved in the oil phase could start becoming destabilized at the depth of nearly 1600 m. The concentration changes displayed two distinct transitions ($d_1$ and $d_2$) as a function of the well depth for this system, which was the result of variation in the amount of stable asphaltene at different $P$ and $T$ conditions following kinetic equations. This transition was observed during all production times at various depths with different slopes, but the initial concentration change ($d_0$−$d_1$) was more equally pronounced at all times, which was reasonable according to the low amount of asphaltene deposition near the upper onset line. After the depth of around 1400 m ($d_1$), at the outset, the destabilization of asphaltene was fast and steep, which was due to the fast

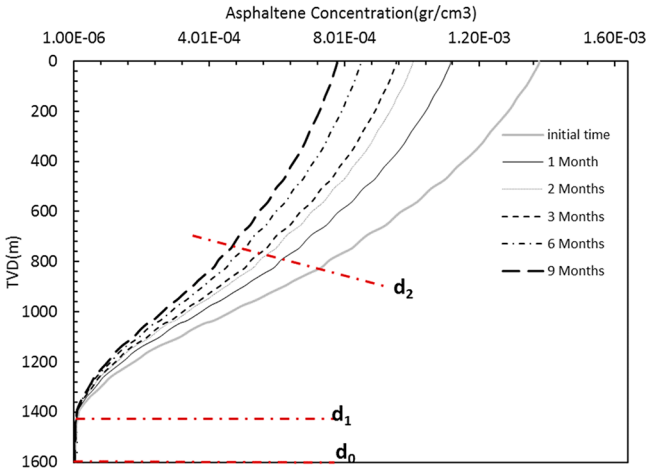


**Figure 8.** Asphaltene concentration change along the depth of the wellbore for different production times.

change in the temperature and pressure of the flow. It is worth noting that the results given in Figure 8 were consistent with those reported as Figure 4 for the temperature and pressure profiles of the vertical flow from the reservoir to the wellhead. Starting from a depth of around 800 m ($d_2$), the trend of destabilized asphaltene slowed, which showed a possible increase in the deposition of asphaltene already destabilized but suspended in the bulk of flow. Additionally, more deposition could result in less difference in the concentration from equilibrium state, and this could also explain the lower destabilization rate. The situation was exacerbated over the production life and showed that the system was more susceptible to asphaltene deposition at the wellhead and near the wellhead region. Also, a decrease in the amount of the precipitated asphaltene over time could be explained by the change in the pressure−temperature conditions of the wellbore, reducing the asphaltene phase fraction at the equilibrium state. In addition, the previously discussed reduction in the asphaltene deposition rate can be explained by the reduction in the precipitated asphaltene amount after 9 months, reducing the deposition rate according to eq 21.

Panels a−d of Figures 9 and 10 show the weight percent of destabilized and suspended asphaltene particles precipitated out of the bulk flow in each group with different particle sizes, as described in Table 1, along the wellbore (a) and on the selected depths (b−d) at the initial flow rate and after 9 months of production, respectively. As seen from Figures 9a and 10a, the percentage of nanoaggregates (group 1) decreases along the well column. In fact, these particles significantly tended to become aggregated and formed larger aggregates. Some of the nanoaggregates can also deposit on the well column wall. Larger aggregates started increasing at the depth of nearly 1600 m and reached a plateau at approximately 800 m depth of the well column (see particle size distribution at this depth in Figures 9c and 10c). In particular, it was possible to recognize three main regimes for groups 2−11 along the wellbore, i.e., an initial rapid increase of the mass percent followed by a slow decrease, which eventually evolved into a final plateau. Largest aggregates, formed as group 12, could not deposit on the well column wall, while smaller aggregates had higher potential to become deposited on the production tubing wall. In general, the same trend, as observed in the initial flow rate, can be seen after 9 months of production. However, it should be mentioned


DOI: 10.1021/acs.energyfuels.7b02714
Energy Fuels 2018, 32, 2661−2672

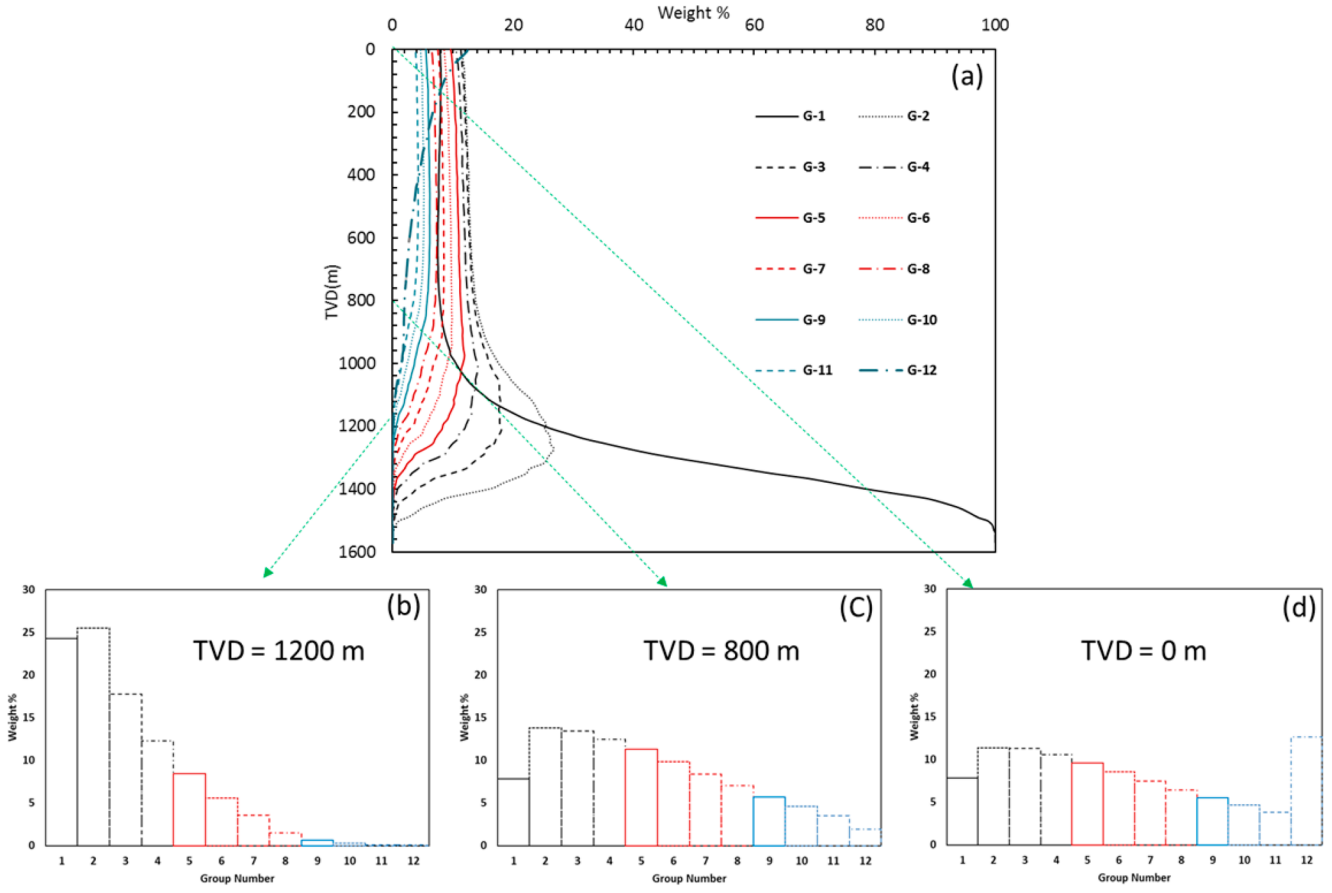


**Figure 9.** Asphaltene particle size classification (a) along the depth of the wellbore, (b) on the depth of 1200 m, (c) on the depth of 800 m, and (d) on the depth of 0 m at the initial flow of the production.

that, as expected, after 9 months, the aggregate sizes decreased along the well column. It is also worth noting that the minimum amount of group 1 along the wellbore after 9 months is substantially higher than that for the initial time, whereas, for group 12, graphs showed the opposite pattern. The possible reason for this behavior is that, owing to a lower precipitated asphaltene concentration after 9 months (Figure 8), the asphaltene aggregation rate reduces according to eq 12, which will keep the fraction of group 1 at a higher state and that of group 12 at a lower state.

Figure 11 shows the variation and distribution of asphaltene particles with different sizes along the well column at various time periods in depositing (groups 1−11) and overall (groups 1−12) forms. As seen, more deposition could occur with the asphaltene particles with smaller sizes. This can be justified by the fact that the smaller aggregates have larger diffusion coefficients and, therefore, move toward the pipeline wall more quickly and could become deposited on the surface. It can be observed that the graphs for depositing particles reached a plateau after an initial increase, indicating the equality between precipitation and consumption of these particles at both deposition and forming group 12. Here, the beginning of the plateau depth was reasonably the same as those reported in Figures 9 and 10. Because the average particle size depends upon both the number of particles and particle size, these results indicated that group 12 had a major role in increasing the overall particle size above the depth of 1200 m (panels b−d of Figures 9 and 10). Finally, it can be seen that the average size at the initial time was higher compared to that after 9 months. These results highlight the previously deduced effect of the aggregation rate change corresponding to the amount of precipitated asphaltenes.

**3.2. Capillary Tube Experiments.** The developed model for the prediction of the asphaltene deposition rate on a steel surface was validated with the experimental data reported in the literature.[32,45] The asphaltene deposition test, performed at the New Mexico Institute of Mining and Technology, was used to assess the predictive capability of the new model. All of the parameters, including the SARA data, crude oil density, diameter, length of the capillary tube, and flow rate of crude oil and pentadecane solution, were reported.[32,45] The asphaltene deposition profile along the capillary length of the pipe was obtained and presented as Figure 12a. The deposition flux profile revealed that the amount of asphaltene deposition was at a maximum at the beginning of the capillary tube as a result of the maximum concentration driving force at these areas. The asphaltene deposition was reduced along the axial length of the capillary tube as the amount of asphaltene aggregates in the flowing crude oil/precipitant solution decreased. The comparison of the results from the developed model to the experimental data found in the experiments of Wang and Buckly[45] and Kurup et al.[32] is shown in Figure 12a. It should be stated that the kinetic parameters were determined by matching the data for the peak of the asphaltene deposition flux obtained by simulations with the experimental data. In this set of experiments, the temperature of the system was kept constant and the pressure change was not noticeable along the axial length of the tube. As seen, the results obtained from the



DOI: 10.1021/acs.energyfuels.7b02714
Energy Fuels 2018, 32, 2661−2672

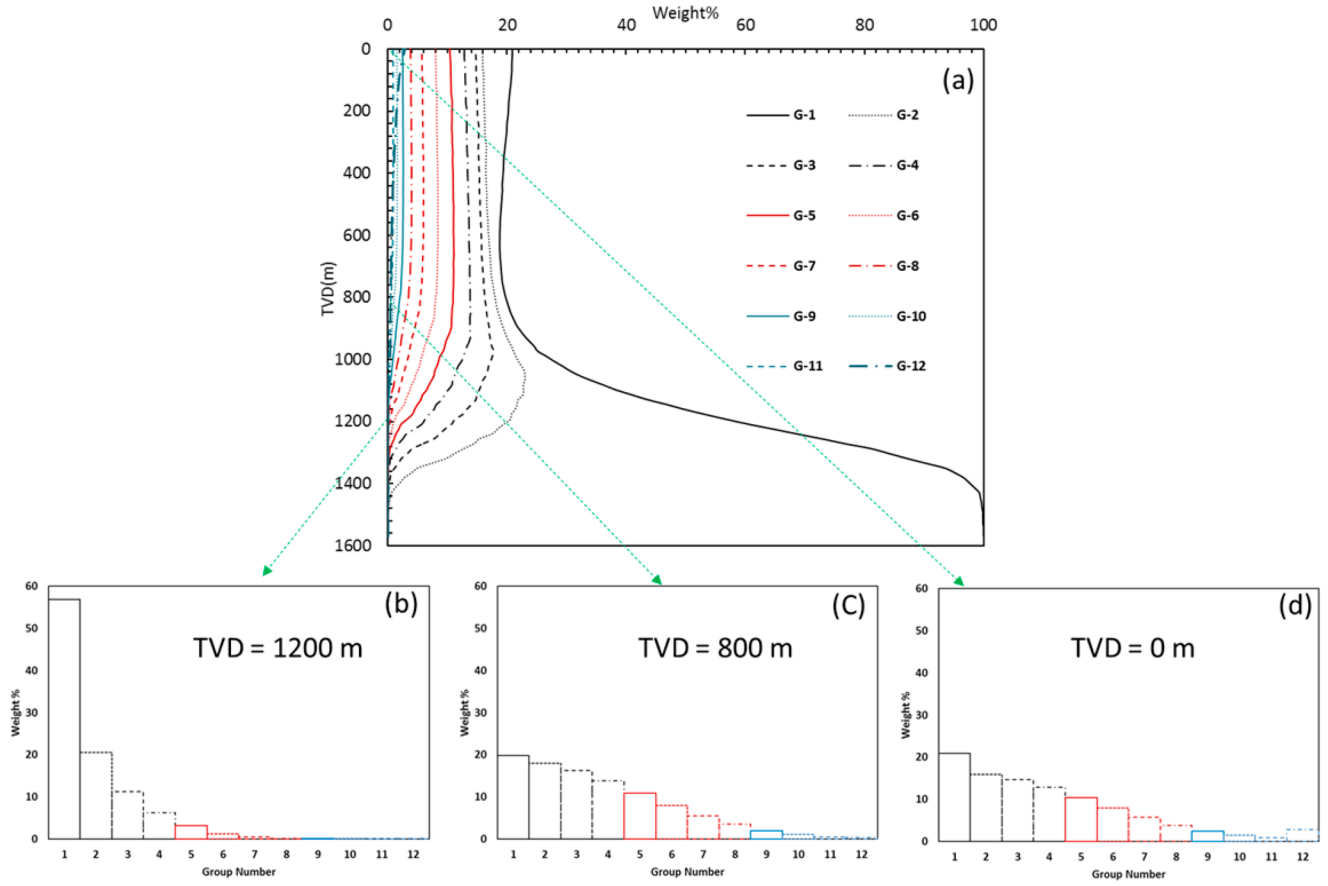


**Figure 10.** Asphaltene particle size classification (a) along the depth of the wellbore, (b) on the depth of 1200 m, (c) on the depth of 800 m, and (d) on the depth of 0 m after 9 months of production.

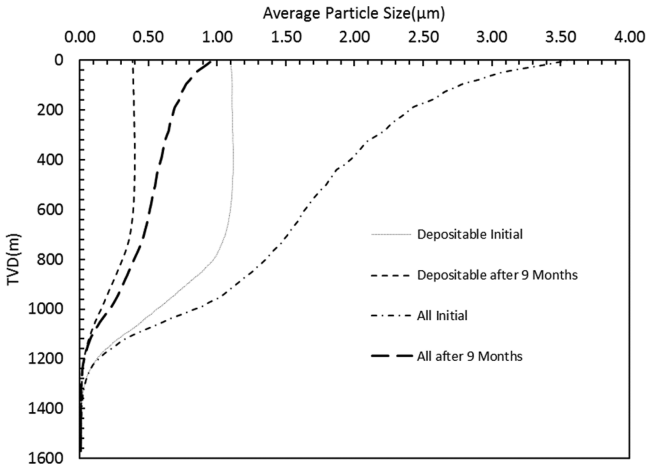


**Figure 11.** Average asphaltene particle size distribution along the depth of the wellbore for different production times.

new model were thoroughly consistent with the experimental results. Another capillary tube deposition experiment was conducted with different operating conditions using the same crude oil/pentadecane solution as explained for the previous test. The aim of the second test was to investigate the effect of a change in operating conditions on the asphaltene deposition flux in the capillary test tube. The tube used in this set of experiments had a larger diameter, and the experiment was performed at a higher flow rate of the oil/precipitant solution. The asphaltene deposition flux profile along the capillary length of the pipe was presented in Figure 12b (solid black data points). It can be observed that, for a larger diameter capillary tube and higher flow rate, a relatively higher magnitude of asphaltene deposition can be seen compared to the deposition flux in a thinner tube and at lower flow rates (Figure 12a). A larger diameter tube and higher flow rate resulted in a higher amount of asphaltene mass flux into the pipe, allowing more asphaltene particles to be unstable and precipitate out of the solution, ready to be deposited onto the pipe surface, and therefore made an increase in the asphaltene deposition accordingly. The results of the new model were compared to this set of experimental data. Because the same oil/precipitant solution was used in the second set and the temperature and the other conditions all remained constant, hence, the same kinetic parameters were used for the asphaltene prediction as explained in the case of the first comparison. Once again, it can be seen from this comparison that the new model can accurately predict the experimental data.

## 4. CONCLUSION

A new dynamic and two-dimensional particle-scale model was developed in this work to simulate the asphaltene deposition in a synthetic oil well. The model could explain the effect of the asphaltene particle size in the aggregation and deposition of asphaltene on the well tubing wall. It was shown that the asphaltene aggregates tended to interact with each other as a result of the Brownian motion and formed larger particles, and therefore, this fact was taken into account in the asphaltene deposition model by considering the variation of the asphaltene


DOI: 10.1021/acs.energyfuels.7b02714
Energy Fuels 2018, 32, 2661−2672

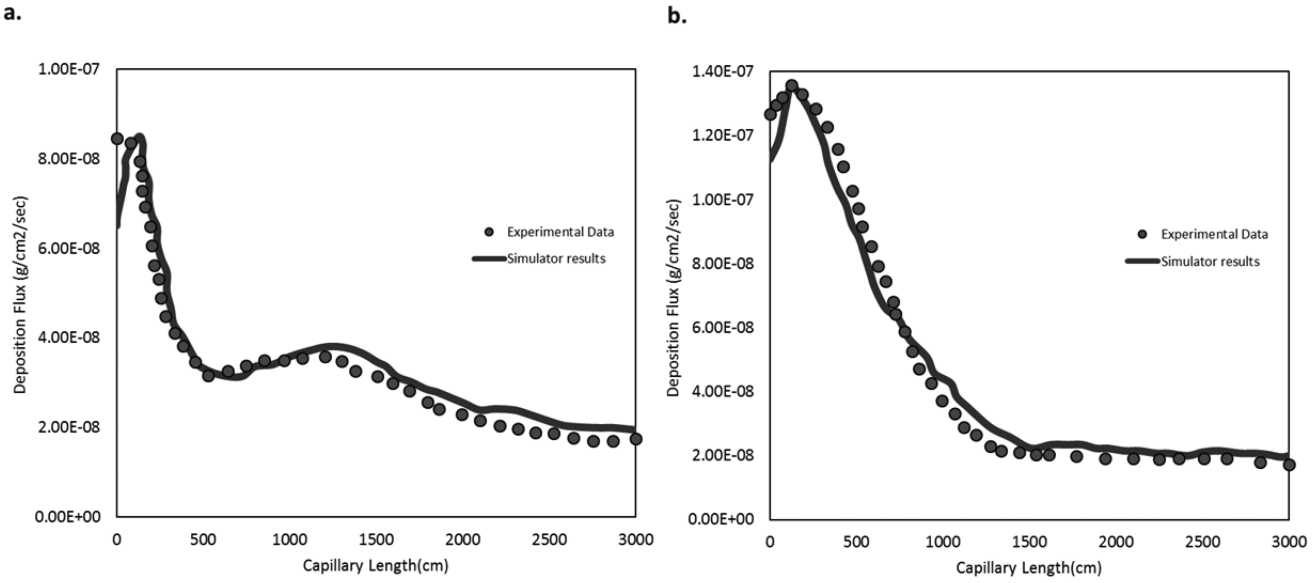


**Figure 12.** Comparison of the results obtained from the model with the asphaltene deposition experimental data in a capillary tube for (a) test 1 and (b) test 2.

particle size during the oil flow along the flowline. It was also concluded that smaller aggregates had a higher tendency to deposit on the tubing wall as a result of the large radial diffusivity of the particles. The results showed that the amount of asphaltene deposition along with the rate of asphaltene deposition strongly depended upon the production time, and it was concluded that both the amount and rate of asphaltene deposition reduced over time. The results obtained from the new model were compared to those reported in the literature, and good agreement between the results was observed. In the modeling of the crude oil phase behavior, an accurate and reliable EoS was employed to characterize the phase behavior of oil/asphaltene/gas systems. It should be stated that all thermodynamic parameters used in the model directly emanated from the published literature. The capability in predicting the experimental results associated with the numerical features, including the computation time, could be considered as the clearest advantages of the new model developed in this work.

## ■ ASSOCIATED CONTENT

### Supporting Information

The Supporting Information is available free of charge on the ACS Publications website at DOI: 10.1021/acs.energyfuels.7b02714.

Numerical method (PDF)

## ■ AUTHOR INFORMATION


### Corresponding Author

*E-mail: ah63@hw.ac.uk.

### ORCID

Aliakbar Hassanpouryouzband: 0000-0003-4183-336X

Antonin Chapoy: 0000-0002-1368-5091


### Notes

The authors declare no competing financial interest.

## ■ NOMENCLATURE

$\tilde{a}$ = Helmholtz free energy

$\tilde{a}^{hc}$ = hard-chain reference contribution to Helmholtz free energy

$\tilde{a}^{disp}$ = dispersion contribution to Helmholtz free energy

$\tilde{a}^{res}$ = residual Helmholtz free energy

$C$ = concentration of asphaltene

$C_{BH}$ = concentration of asphaltene at bottomhole

$C_k$ = concentration of particle size $k$

$C_f$ = concentration of asphaltene in the oil phase

$C_{eq}$ = concentration of asphaltene at equilibrium conditions

$D_{wo}$ = asphaltene diffusivity coefficient in the oil phase

$f_d$ = diffusivity coefficient tuning parameter

$f_F$ = friction factor

$g$ = acceleration due to gravity

$h_o$ = convective heat transfer coefficient of oil

$k$ = asphaltene size group number

$k_{As}$ = thermal conductivity of asphaltene

$k_B$ = Boltzmann constant

$k_d$ = asphaltene deposition rate constant

$k_p$ = precipitation rate constant

$k_0$ = precipitation rate constant tuning parameter

$k_C$ = thermal conductivity of casing

$L$ = length of capillary/wellbore

$n_d$ = adjustable parameter for the proposed deposition model

$N_{Re}$ = Reynolds number

$P$ = pressure

$P_{res}$ = reservoir pressure

$P_{WH}$ = wellhead pressure

$r$ = radius

$r_w$ = wellbore/capillary radius

$r_k$ = radius of particle size $k$

$R$ = rate of production and consumption of precipitated asphaltene

$R_{per}$ = rate of asphaltene precipitating out of the oleic phase

$R_d$ = rate of asphaltene deposition

$t$ = time

$T$ = temperature

$T_{res}$ = reservoir temperature

$T_{WH}$ = wellhead temperature

$T_o$ = oil temperature

$V_r$ = radial velocity



DOI: 10.1021/acs.energyfuels.7b02714
Energy Fuels 2018, 32, 2661−2672

$V_z$ = axial velocity
$V_\theta$ = angular velocity
$x_i$ = composition of species $i$
$z$ = axial length
$Z$ = compressibility factor

### Greek Letters

$\alpha_p$ = precipitation rate constant tuning parameter
$\alpha_T$ = thermal diffusivity
$\beta$ = collision efficiency
$\varepsilon$ = relative roughness
$\varepsilon_h$ = turbulent heat diffusivity
$\varepsilon_m$ = turbulent mass diffusivity
$\eta$ = viscosity
$\eta^*$ = viscosity of dilute gas
$\eta_p$ = packing fraction
$\theta$ = angle
$\mu_k^{res}$ = residual chemical potential
$\nu_\nu$ = mean friction velocity
$\nu_\mu$ = kinematic viscosity
$\nu_\nu$ = molar volume
$\xi$ = viscosity-reducing parameter
$\rho$ = density
$\rho_r$ = reduced density
$\rho_n$ = total number density of molecules
$\varphi_k$ = fugacity coefficient
$\phi$ = volume fraction of asphaltene particles

## REFERENCES


(1) Adams, J. J. *Energy Fuels* **2014**, *28* (5), 2831−2856.
(2) Mullins, O. C. Optical Interrogation of Aromatic Moieties in Crude Oils and Asphaltenes. In *Structure and Dynamics of Asphaltenes*; Mullins, O. C., Sheu, E. Y., Eds.; Springer: Boston, MA, 1998; Chapter 2, pp 21−77, DOI: 10.1007/978-1-4899-1615-0_2.
(3) Speight, J. G.; Moschopedis, S. E. On the Molecular Nature of Petroleum Asphaltenes. In *Chemistry of Asphaltenes*; Bunger, J. W., Li, N. C., Eds.; American Chemical Society (ACS): Washington, D.C., 1981; Advances in Chemistry, Vol. *195*, Chapter 1, pp 1−15, DOI: 10.1021/ba-1981-0195.ch001.
(4) Joonaki, E.; Hassanpouryouzband, A.; Burgass, R.; Tohidi, B. Effect of Water Chemistry on Asphaltene Stabilised Water in Oil Emulsions—A New Search for Low Salinity Water Injection Mechanism. *Proceedings of the 79th EAGE Conference and Exhibition 2017*; Paris, France, June 12−15, 2017; DOI: 10.3997/2214-4609.201701297.
(5) Wang, M.; Hao, Y.; Islam, M. R.; Chen, C. C. *AIChE J.* **2016**, *62* (4), 1254−1264.
(6) Yarranton, H. W.; Masliyah, J. H. *AIChE J.* **1996**, *42* (12), 3533−3543.
(7) Hassanpouryouzband, A.; Kor, P.; Joonaki, E.; Taghikhani, V.; Bozorgmehry Boozarjomehry, R.; Chapoy, A. Development of a New Model for Quantifying of Asphaltene Deposition—Role of Precipitation, Aggregation and Radial Transport. *Proceedings of the 79th EAGE Conference and Exhibition 2017*; Paris, France, June 12−15, 2017; DOI: 10.3997/2214-4609.201700755.
(8) Eskin, D.; Mohammadzadeh, O.; Akbarzadeh, K.; Taylor, S. D.; Ratulowski, J. *Can. J. Chem. Eng.* **2016**, *94* (6), 1202−1217.
(9) Escobedo, J.; Mansoori, G. Asphaltene and Other Heavy-Organic Particle Deposition during Transfer and Production Operations. *Proceedings of the SPE Annual Technical Conference and Exhibition*; Dallas, TX, Oct 22−25, 1995; pp 343−358; DOI: 10.2118/30672-MS.
(10) Paes, D. M.; Ribeiro, P. R.; Shirdel, M.; Sepehrnoori, K. *J. Pet. Sci. Eng.* **2015**, *129*, 77−87.
(11) Jamialahmadi, M.; Soltani, B.; Müller-Steinhagen, H.; Rashtchian, D. *Int. J. Heat Mass Transfer* **2009**, *52* (19), 4624−4634.
(12) Soltani Soulgani, B.; Rashtchian, D.; Tohidi, B.; Jamialahmadi, M. *J. Jpn. Pet. Inst.* **2009**, *52* (6), 322−331.
(13) Ramirez-Jaramillo, E.; Lira-Galeana, C.; Manero, O. *Energy Fuels* **2006**, *20* (3), 1184−1196.
(14) Kern, D. Q.; Seaton, R. E. *Br. Chem. Eng.* **1959**, *4* (5), 258−262.
(15) Burger, E. D.; Perkins, T. K.; Striegler, J. H. *JPT, J. Pet. Technol.* **1981**, *33* (06), 1075−1086.
(16) Greaves, M.; Ayatollahi, S.; Moshfeghian, M.; Alboudwarej, H.; Yarranton, H. W. *J. Can. Pet. Technol.* **2004**, *43* (09), 31−39.
(17) Eskin, D.; Ratulowski, J.; Akbarzadeh, K.; Andersen, S. *AIChE J.* **2012**, *58* (9), 2936−2948.
(18) Vargas, F. M.; Creek, J. L.; Chapman, W. G. *Energy Fuels* **2010**, *24* (4), 2294−2299.
(19) Hashmi, S. M.; Loewenberg, M.; Firoozabadi, A. *Phys. Fluids* **2015**, *27* (8), 083302.
(20) Vilas Bôas Fávero, C.; Hanpan, A.; Phichphimok, P.; Binabdullah, K.; Fogler, H. S. *Energy Fuels* **2016**, *30* (11), 8915−8921.
(21) Elimelech, M.; Gregory, J.; Jia, X.; Williams, R. A. Modelling of aggregation processes. *Particle Deposition & Aggregation*; Elsevier: Amsterdam, Netherlands, 1995; Chapter 6, pp 157−202, DOI: 10.1016/B978-075067024-1/50006-6.
(22) Barker, J. A.; Henderson, D. *J. Chem. Phys.* **1967**, *47* (11), 4714−4721.
(23) Gross, J.; Sadowski, G. *Ind. Eng. Chem. Res.* **2001**, *40* (4), 1244−1260.
(24) Michelsen, M. L. *Fluid Phase Equilib.* **1982**, *9* (1), 1−19.
(25) Michelsen, M. L. *Fluid Phase Equilib.* **1982**, *9* (1), 21−40.
(26) Michelsen, M. L. *Comput. Chem. Eng.* **1994**, *18* (7), 545−550.
(27) Gupta, A. K.; Raj Bishnoi, P.; Kalogerakis, N.; Bishnoi, R. *Fluid Phase Equilib.* **1991**, *63*, 65−89.
(28) Panuganti, S. R.; Tavakkoli, M.; Vargas, F. M.; Gonzalez, D. L.; Chapman, W. G. *Fluid Phase Equilib.* **2013**, *359*, 2−16.
(29) Jossi, J. A.; Stiel, L. I.; Thodos, G. *AIChE J.* **1962**, *8* (1), 59−63.
(30) Lohrenz, J.; Bray, B. G.; Clark, C. R. *JPT, J. Pet. Technol.* **1964**, *16* (10), 1171−1176.
(31) Brinkman, H. C. *J. Chem. Phys.* **1952**, *20* (4), 571.
(32) Kurup, A. S.; Vargas, F. M.; Wang, J.; Buckley, J.; Creek, J. L.; Subramani, J. H.; Chapman, W. G. *Energy Fuels* **2011**, *25* (10), 4506−4516.
(33) Maqbool, T.; Raha, S.; Hoepfner, M. P.; Fogler, H. S. *Energy Fuels* **2011**, *25* (4), 1585−1596.
(34) Vilas Bôas Fávero, C.; Maqbool, T.; Hoepfner, M.; Haji-Akbari, N.; Fogler, H. S. *Adv. Colloid Interface Sci.* **2017**, *244*, 267−280.
(35) Seifried, C. M.; Crawshaw, J.; Boek, E. S. *Energy Fuels* **2013**, *27* (4), 1865−1872.
(36) Cengel, Y. A.; Cimbala, J. M. *Fluid Mechanics Fundamentals and Applications*; McGraw-Hill Korea: Seoul, Korea, 2006.
(37) Edward, J. T. *J. Chem. Educ.* **1970**, *47* (4), 261.
(38) Datta, A. K. *Biological and Bioenvironmental Heat and Mass Transfer*; CRC Press: Boca Raton, FL, 2002; DOI: 10.1201/9780203910184.
(39) Singh, P.; Venkatesan, R.; Fogler, H. S.; Nagarajan, N. *AIChE J.* **2000**, *46* (5), 1059−1074.
(40) Whitaker, S. *Transp. Porous Media* **1986**, *1* (1), 3−25.
(41) Chen, N. H. *Ind. Eng. Chem. Fundam.* **1979**, *18* (3), 296−297.
(42) Zheng, S.; Saidoun, M.; Palermo, T.; Mateen, K.; Fogler, H. S. *Energy Fuels* **2017**, *31* (5), 5011−5023.
(43) Gonzalez, D. L.; Ting, P. D.; Hirasaki, G. J.; Chapman, W. G. *Energy Fuels* **2005**, *19* (4), 1230−1234.
(44) David Ting, P.; Hirasaki, G. J.; Chapman, W. G. *Pet. Sci. Technol.* **2003**, *21* (3−4), 647−661.
(45) Wang, J.; Buckley, J. S.; Creek, J. L. *J. Dispersion Sci. Technol.* **2004**, *25* (3), 287−298.



DOI: 10.1021/acs.energyfuels.7b02714
*Energy Fuels* 2018, 32, 2661−2672